Journal of Mathematical Chemistry 19 (1996) 271–287

Chemical front initiation and propagation in the bromate–ferroin reaction

J.H. Merkin [a], A.J. Poole [a,b] and S.K. Scott [b]

[a] *Department of Applied Mathematical Studies, University of Leeds, Leeds LS2 9JT, UK*
[b] *School of Chemistry, University of Leeds, Leeds LS2 9JT, UK*

Received 1 February 1996

The initiation and propagation of chemical wave fronts in the bromate–ferroin reaction is considered numerically using a two- variable model derived from a reduced version of the FKN mechanism. The results indicate that for a given initial concentration of bromide ion, there is a critical size for the region in which the wave is initiated and that this critical size increases with $[Br^-]_0$. For successful wave initiations, an approximately constant-form travelling reaction wave develops, but the wave speed does not approximate to a constant value in general, indicating that care is required when using experimental data to estimate diffusion coefficients. These observations are also fully consistent with the experimental observations that initiation becomes possible in this reaction after some initiation period that depends inversely on $[BrO_3^-]$ and $[H^+]^2$, the concentrations of bromate and H^+ ions, and logarithmically on $[Br^-]_0$. Initiation becomes more difficult as the space dimension of the system is increased. Analytical estimates based on the assumption of high $[Br^-]_0$ suggest that the critical size scales as $[Br^-]_0^{1/4}$ and that the critical size for 1D, 2D and 3D domains goes in the ratio $1 : 1/\sqrt{2} : 1/\sqrt{3}$.

1. Introduction

The bromate–ferroin reaction [1,2] can be regarded as the inorganic subset of the Belousov–Zhabotinsky (BZ) reaction, lacking the clock-resetting Process C. It is an autocatalytic system in its own right and, in well-stirred closed reactors supports clock reaction behaviour with a relatively sharp oxidation process (and consequent red to blue colour change) occurring after an induction period. The induction period is characterized by the decrease in the bromide ion concentration in a typically pseudo-first order process during which the species $HBrO_2$ is maintained at a low steady state concentration. The induction period ends when $[Br^-]$ falls to a critical value given by

$$[Br^-]_{cr} = \frac{k_5}{k_2}[BrO_3^-], \tag{1}$$

where k_2 and k_5 are rate constants for competing reactions for $HBrO_2$, see mechanism below. At the end of the induction period, the reaction switches to an autocata-

lytic growth in $[HBrO_2]$. The duration of the induction period or 'clock time' t_{cl} has been determined to be [3]

$$t_{cl} = \frac{1}{2k_3[BrO_3^-]_0[H^+]^2} \ln\left\{\frac{k_2[Br^-]_0}{2k_5[BrO_3^-]_0}\right\} \tag{2}$$

provided the initial bromide ion concentration $[Br^-]_0$ is low compared to the initial bromate ion concentration (so that the consumption of the latter can be neglected). For high $[Br^-]_0$, this form can be corrected to give

$$t_{cl} = \frac{1}{k_3\left(2 - \frac{[Br^-]_0}{[BrO_3^-]_0}\right)[BrO_3^-]_0[H^+]^2} \ln\left\{\frac{k_2[Br^-]_0}{2k_5[BrO_3^-]_0}\right\}. \tag{3}$$

These predictions have been confirmed quantitatively by experiment [3].

If the reaction mixture is spread as a thin layer in a petri dish, an oxidation event can be initiated locally with a positively-biased Ag electrode, which is generally assumed to deplete the local bromide ion concentration. Under some conditions, the reaction event may then propagate as a reaction– diffusion front visualised as a blue circle of growing radius spreading into the red (reduced state) ahead of the wave until the basic clock reaction takes over and the whole system turns blue. Showalter [1] has determined many of the appropriate experimental features of this system, including the dependence of the apparent wave velocity on the initial concentrations of the major reactant species (H^+, BrO_3^-, ferroin and the organic species added to prevent the accumulation of Br_2) and the 'wave initiation time', i.e. the time from the initial mixing of the reagents to the first successful initiation of an oxidation wave with the Ag electrode. In this paper, we use the basic inorganic chemistry of the Field–Körös–Noyes (FKN) mechanism [4] to account for these observations both qualitatively and quantitatively.

2. Mechanism and governing equations

The appropriate steps from the FKN mechanism for the bromate–ferroin system are:

Process A: removal of bromide ion

(FKN3) $BrO_3^- + Br^- + 2H^+ \rightarrow HBrO_2 + HOBr$, rate $= k_3[H^+]^2[BrO_3^-][Br^-]$,

(FKN2) $HBrO_2 + Br^- + H^+ \rightarrow 2HOBr$, rate $= k_2[H^+][HBrO_2][Br^-]$,

so, overall this has the stoichiometry

Process A: $BrO_3^- + 2Br^- + 3H^+ \rightarrow 3HOBr$.

Process B: autocatalysis and oxidation

(FKN5) $BrO_3^- + HBrO_2 + H^+ \rightarrow 2BrO_2 + H_2O$, rate $= k_5[BrO_3^-][H^+][HBrO_2]$,

(FKN6) $BrO_2 + M_{red} + H^+ \rightarrow HBrO_2 + M_{ox}$, rate $= k_6[BrO_2][M_{red}][H^+]$.

The radical intermediate species BrO_2 reacts rapidly by step (FKN6) if the catalyst (represented by M_{red}) is ferroin, so these two steps give rise to the overall stoichiometry

Process B: $BrO_3^- + HBrO_2 + 3H^+ + 2M_{red} \rightarrow 2HBrO_2 + 2M_{ox} + H_2O$

with (FKN5) being the rate determining step. This autocatalysis in $HBrO_2$ also brings about the oxidation of the redox catalyst. As the $HBrO_2$ concentration increases, the following reaction

(FKN4) $2HBrO_2 \rightarrow BrO_3^- + HOBr + H^+$, rate $= k_4[HBrO_2]^2$,

becomes important in limiting the growth of the autocatalyst.

The concentrations of the major reactants, BrO_3^-, H^+ and M_{red} (the reduced, ferroin form of the redox catalyst) will be taken as constants in this study with BrO_2 eliminated by assuming it is in a steady state between steps (FKN5) and (FKN6). The governing reaction–diffusion equations for $[HBrO_2]$ and $[Br^-]$ can be written in the following dimensionless forms:

$$\frac{\partial u}{\partial t} = \nabla^2 u + u(1-u) + (q-u)v, \tag{4a}$$

$$\delta\frac{\partial v}{\partial t} = \delta D\nabla^2 v - (q+u)v. \tag{4b}$$

Here $u = 2k_4[HBrO_2]/k_5[H^+][BrO_3^-]$, $v = k_2[Br^-]/k_5[BrO_3^-]$ and $t = k_5[H^+] \times [BrO_3^-]t'$, where t' is the actual (physical time). The parameters $\delta = 2k_4/k_2[H^+]$ and $q = 2k_3k_4/k_2k_5$ with $D = D_u/D_v$, the ratio of the diffusion coefficients of the two species: throughout this work we take the simplest case, $D = 1$, i.e. we assume equal diffusion coefficients for $HBrO_2$ and Br^-. The appropriate length scale is given by $l_{ref} = (D_u/k_5[BrO_3^-[H^+])^{1/2}$ with the distance then being $x = x'/l_{ref}$ etc., where x' is the physical distance. The scalings for u and v and the parameter q are the usual forms for the Oregonator model [5]: the emergence of the parameter δ is discussed in Merkin et al. [3].

In one space dimension, the Laplacian has the simple form $\nabla^2 = \partial^2/\partial x^2$. For the initial conditions, we have taken

$$u(x,0) = q \quad \text{for all } x,$$

and

$$v(x,0) = \begin{cases} v_0 & \text{for } x > \sigma, \\ 0 & \text{for } |x| \leqslant \sigma. \end{cases} \tag{5}$$

This sets the autocatalyst concentration [$HBrO_2$] equal to its pseudo-steady state value everywhere and assumes a (dimensionless) initial bromide ion concentration of v_0 everywhere except in a (narrow) region close to the origin ($|x| \leqslant \sigma$), for which the concentration is set equal to zero as a simplified representation of the effect of a positively biased Ag electrode of dimensionless half-width σ. We also impose the following boundary conditions:

$$\partial u/\partial x = \partial v/\partial x = 0 \quad \text{at } x = 0 \quad \text{(symmetry)}, \tag{6a}$$

$$\partial u/\partial x = \partial v/\partial x \to 0 \quad \text{as } x \to \infty. \tag{6b}$$

In higher space dimensions, we expect circular or spherically symmetric waves from symmetric initial conditions and so can cast the governing equations in terms of the dimensionless radial co-ordinate r with $\nabla^2 = (j/r)(\partial/\partial r) + (\partial^2/\partial r^2)$ and $j = 1$ and 2 for circular and spherical domains, respectively; the initial and boundary conditions are as above with r replacing x.

3. Numerical results

Subject to the above initial and boundary conditions, eqs. (4a, b) were solved numerically using a method similar to that described in [6]. Basically, the scheme implements a Crank–Nicolson method in which the time derivates are replaced by forward differences and all other terms are averaged over the t to $t + \Delta t$ timestep. This results in two coupled ordinary differential equations in x in which the derivatives are approximated by central finite differences. Newton–Raphson iteration is then implemented to solve the resulting systems of nonlinear algebraic equations that are formed at each step. The time step used in the code was adjustable in order to maintain a prescribed degree of accuracy. In the numerical results presented below, the parameters D, δ and q were fixed at 1.0, 0.01 and 0.0001, respectively.

3.1. 1D GEOMETRY: INITIATION OF TRAVELLING WAVES

The local depletion of the concentration v of the inhibitor species (Br^-) as expressed by the initial condition (5) allows the autocatalytic Process B to develop, as expressed by the $u(1 - u)$ term in eq. (4a). This kinetic growth, however, must compete with the regrowth of v due to diffusion from the surrounding region (in which v is typically relatively high). The competition is complicated by two additional features: the bromide ion concentration in the surrounding region falls spontaneously due to the clock reaction, reducing the driving force for the diffusion of the inhibitor, whilst the increasing concentration of autocatalyst u enhances the kinetic removal of the bromide ion in the 'interface' between the two regions. The competition between the growth and inhibition depends primarily on the two parameters σ and v_0, the half-width of the initiation region and the surrounding

initial inhibitor concentration. The larger the value of σ, the longer it takes for diffusion to restore the bromide ion concentration close to the origin to a value close to the critical bromide ion concentration ($v = 1$ in the present scaling) and, hence, the longer the clock process takes to reduce the bulk bromide ion concentration. We may then expect the development of the autocatalytic process to be favoured by large σ or low initial bromide ion concentrations v_0.

Fig. 1 compares the development of two similar computations, each with $v_0 = 6000$, a typical experimental value, but differing in the value of σ. The results are presented by colouring positions for which $u < 1/2$ red and those with $u > 1/2$ blue (this choice approximates the experimental observations corresponding to reduced and oxidised regions).

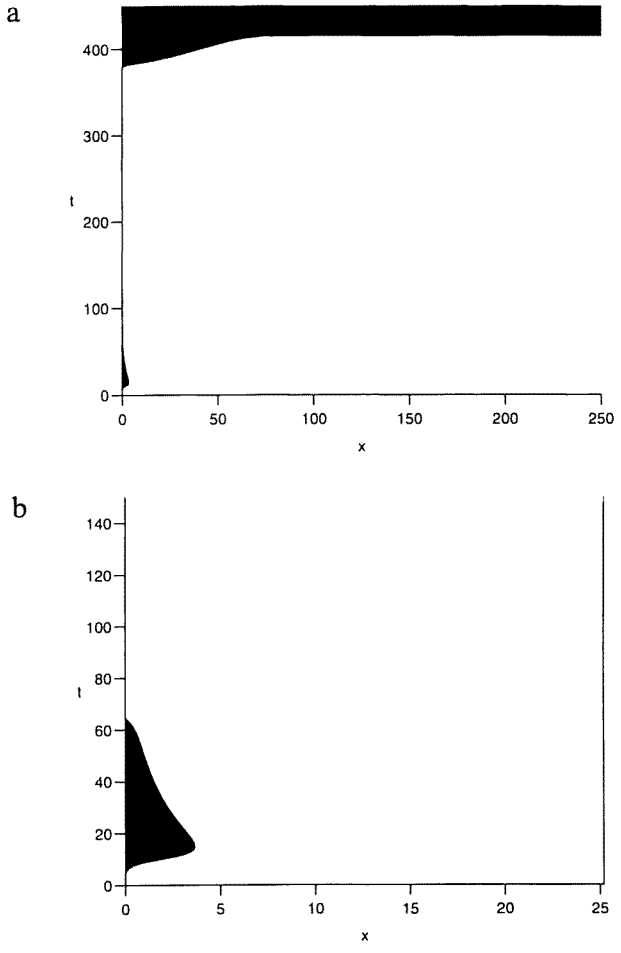

Fig. 1. Comparison of the development of the long and short time behaviour of two computations, each with $v_0 = 6000$. (a) and (b) depict the front development, and subsequent inhibition, for the case when $\sigma = 16.6$, whilst (c) and (d) show the case for $\sigma = 16.7$, where a front is able to propagate. *Fig. 1 continued on next page.*

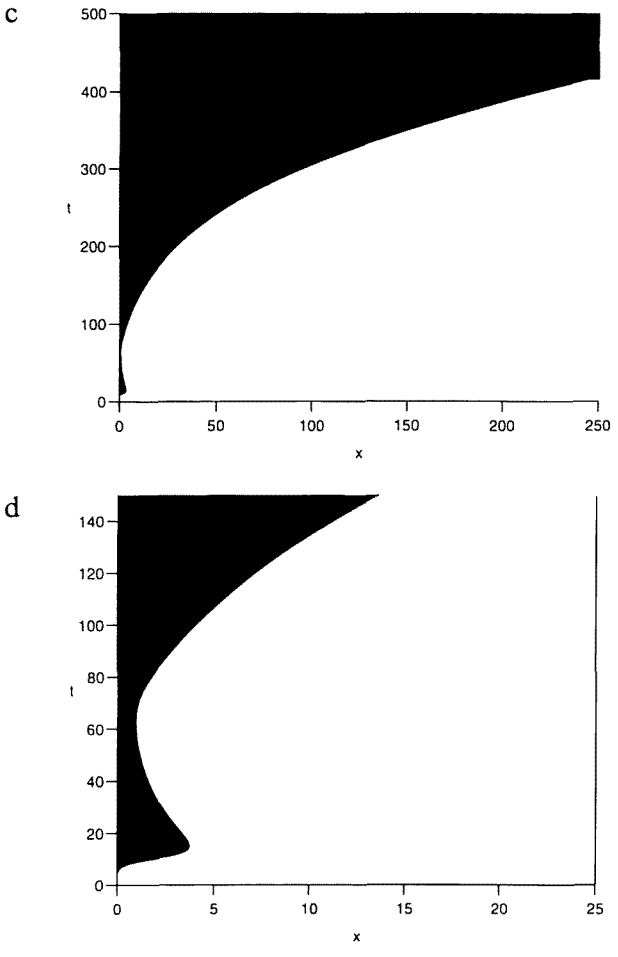

Fig. 1 (continued).

In each case the whole reaction zone is initially in the reduced state, but the removal of the autocatalyst over the region $0 \leqslant x \leqslant \sigma$ allows the autocatalytic process to begin. If there were no diffusion of inhibitor back into the initiation region, the red to blue colour change would develop after a short period (approximately $-\ln(q) \approx 9.2$ in the dimensionless time variable) in which u grows from its initial value $u = q$ to $u = 1/2$. This evolution can be seen close to $x = 0$, with the red-to-blue oxidation process developing rapidly out to $x \approx 4$, although the development time increases slightly with x, indicating the effect of the re-diffusion of bromide ions back into the region. The diffusion of the inhibitor is such that the autocatalytic oxidation becomes suppressed at longer times for $x > 4$ and the concentration u falls again due to the reactions of Process A. This appears as the red–blue interface moving back towards the origin. For $\sigma = 16.6$, Figs. 1(a, b), the 'front' eventually reaches the origin for $t \approx 65$. There is then a relatively long, apparently dormant

phase before an essentially homogeneous change from the reduced to the oxidised state corresponding to a 'global' clock reaction. Away from the initiation region, the clock time closely corresponds to that predicted by eq. (2), which in dimensionless terms can be written as

$$t_{\mathrm{cl}} = \frac{\delta}{2q} \ln(\tfrac{1}{2} v_0) , \tag{7}$$

giving $t_{\mathrm{cl}} = 400$. Closer to the origin, however, the clock time is somewhat shortened by the initial depletion of the bromide ion, so the red-to-blue 'front' appears to have some 'propagation' across the region $0 < x < \sigma$. The scenario described above corresponds to a failure to initiate a wave, and is simply a slight modification of the homogeneous clock process.

For a slightly larger value of the initiation zone half-width, $\sigma = 16.7$, there is a similar early development, Fig. 1(c), but in this case the diffusion of the inhibitor back into the initiation region and the consequent suppression of Process B do not penetrate back all the way to the origin. Instead, there is a narrow region, approximately $0 < x < 1.5$ for which the change back to low values of u (and hence from blue back to red in the present scheme) does not occur. There, u approaches its final value of 1 and the diffusion of autocatalyst from this region to larger values of x and the subsequent reaction are sufficient to prevent v from reaching its critical value. The autocatalytic oxidation process then propagates as a true reaction–diffusion wave away from this region close to the origin, as shown in Fig. 1(d). (We may also note that just before the wave reaches the end of the system, there is evidence of the remnants of the clock process, with the oxidation process occurring over $240 < x < 250$ almost simultaneously for $t = 400$.)

3.2. CRITICAL INITIATION SIZE

The difference in the behaviour for $\sigma = 16.6$ and 16.7 indicates the possible existence of some'critical' initiation half-width σ_{cr}, with $16.6 < \sigma_{\mathrm{cr}} < 16.7$ for $v_0 = 6000$. The critical half-width has been determined for other values of the bulk initial bromide ion concentration and the $\sigma_{\mathrm{cr}}(v_0)$ locus is shown in Fig. 2(a), with the condition for front initiation lying above this locus and front suppression lying below. The data is replotted in Fig. 2(b) as σ_{cr} versus $v_0^{1/4}$: as set out in the appendix, such a scaling of the critical half-width with the initial bromide ion concentration can be expected for large v_0 and σ simply on the basis of diffusion and the existence of a critical bromide ion concentration. The numerical data for the 1D system do appear to satisfy this scaling at large half-widths although there is, not unexpectedly, considerable departure at small v_0.

For systems with $\sigma \ll \sigma_{\mathrm{cr}}$ a 'total inhibition' can arise, in which the bromide ion concentration at the origin reaches its critical value by diffusion before the autocatalytic process causes u to reach the value 1/2 at any point. There is then just the homogeneous clock process at long time. At the other extreme, for $\sigma \gg \sigma_{\mathrm{cr}}$, the

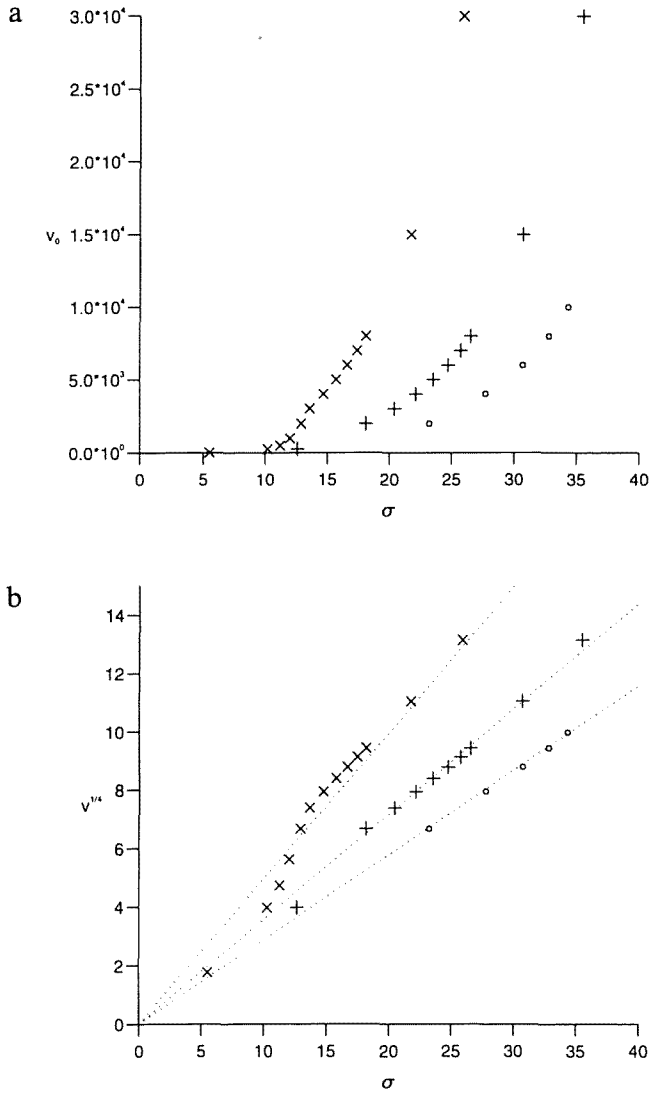

Fig. 2. (a) Numerically computed values of the dependence of the critical initiation size, σ_{cr}, on v_0 for the 1, 2 and 3 dimensional systems. (b) σ_{cr} versus $v_0^{1/4}$.

feature that the initial red-to-blue colour change is restricted to a region somewhat smaller than the whole initiation region persists, as does the period during which the diffusion of v causes the oxidised region to decrease in extent before the full development of the reaction–diffusion front, as indicated in Fig. 3(a), where the locus red–blue interface is shown. This latter aspect is, however, only a feature of systems with high v_0. Fig. 3(b) shows the evolution of this interface for marginally subcritical and supercritical cases ($\sigma = 12.9$ and 13.0, respectively) for $v_0 = 2000$. In this case, the subcritical system again shows the oxidation process occurring over a nar-

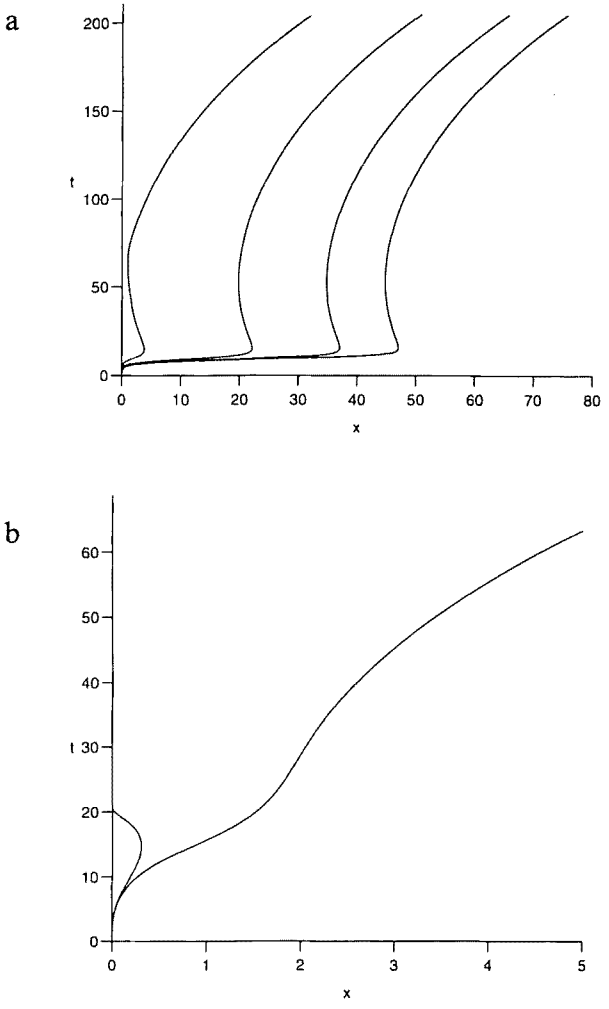

Fig. 3. Comparison of the front development for systems with varying σ. (a) $v_0 = 6000$ and $\sigma = 16.7, 20.0, 35.0, 50.0, 60.0$. (b) $v_0 = 2000$ and $\sigma = 12.9, 13.0$. (c) $v_0 = 2000$ and $\sigma = 13.0, 20.0, 30.0, 40.0$. *Fig. 3 continued on next page.*

row region, but that the diffusion of v and the consequent reduction process move back through the whole zone to reach the origin. In the supercritical case, the initial oxidation process develops into a full reaction–diffusion front without the blue region decreasing in size at any stage. It is possible that a finer examination of the system in the parameter range $12.9 < \sigma < 13.0$ would reveal loci that do have this period of 'reversal' but it is clearly not a dominant feature as it is for higher v_0. Fig. 3(c) shows the interface evolution for larger values of σ, for which there are relatively extended periods in which the interface remains at almost constant x. The equivalent behaviour, with the blue region spending an extended period of approximately constant width is observed experimentally.

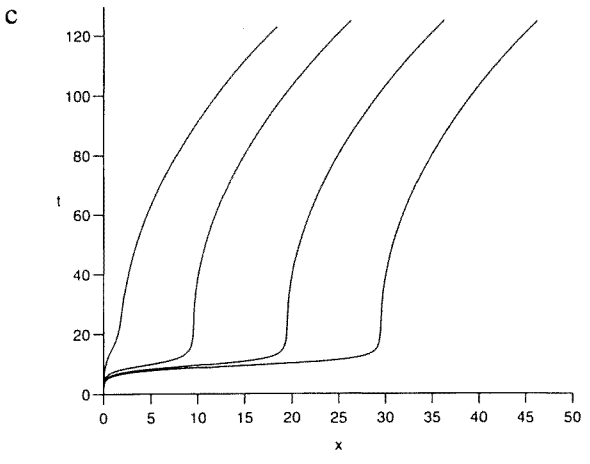

Fig. 3 (continued).

At very low v_0, the clock time can become so short that it becomes difficult to distinguish between the propagation of a reaction–diffusion front and a simple 'phase wave' structure reflecting the spatially inhomogeneous initial bromide ion concentration inherent in eq. (5).

3.3. EVOLUTION OF FRONT VELOCITY

The velocity of the reaction–diffusion front for the system with $v_0 = 6000$ and $\sigma = 16.7$ can be obtained from the inverse of the gradient of the red–blue interface in Fig. 1(d). A constant velocity would correspond to a straight line. Fig. 4(a) indicates the variation of the instantaneous velocity w with time. The velocity is evaluated using central differences from the position x_t at time t and the position two time increments earlier, $t - 2\Delta t$, with the 'position' of the front at any time being determined as $x_t = I/(1 - u_\infty)$ where $I = \int_0^L (u - u_\infty)dx$ with L the length of the numerical integration domain and u_∞ the computed value of u at $x = L$. (L was chosen to be large enough for there to be a sufficiently long region ahead of any reaction–diffusion event in which the concentration gradients can approach zero.) The early evolution gives a sharp peak that is associated with the initial autocatalytic development rather than the true reaction–diffusion front. There is then a sharp fall in the velocity, which actually becomes negative in the above definition as the red–blue interface moves back towards the origin. From $t \approx 90$ onwards, however, the velocity increases steadily as the true reaction–diffusion front moves across the reaction zone. there is a final sharp increase at $t \approx 400$, corresponding to the final clock reaction event ahead of the front.

A similar structure is exhibited for the system with $v_0 = 2000$ and $\sigma = 13.0$, Fig. 4(b), although in this case there is no period of apparent negative velocity and

the initial spike is much reduced. In neither case does the velocity approach a constant value – in fact the linear portions in these figures indicate that the front has more of a constant- acceleration rather than a constant-velocity character. It is also apparent that the velocity does not, at least in these instances, approach the 'expected' Fisher–Kolmogorov wave velocity $w = 2$ (in the present dimensionless variables). The experimental observations [1] support the idea that the velocity in the bromate–ferroin system is not constant, although Showalter did fit a linear position–time dependence to produce wave velocities. It is also common for authors to use the 'expected' results $w = 2$ to derive estimates for diffusion coefficients from such experimentally measured velocities. The reason that the wave velocity is not constant in this system is readily apparent; the spontaneous reaction

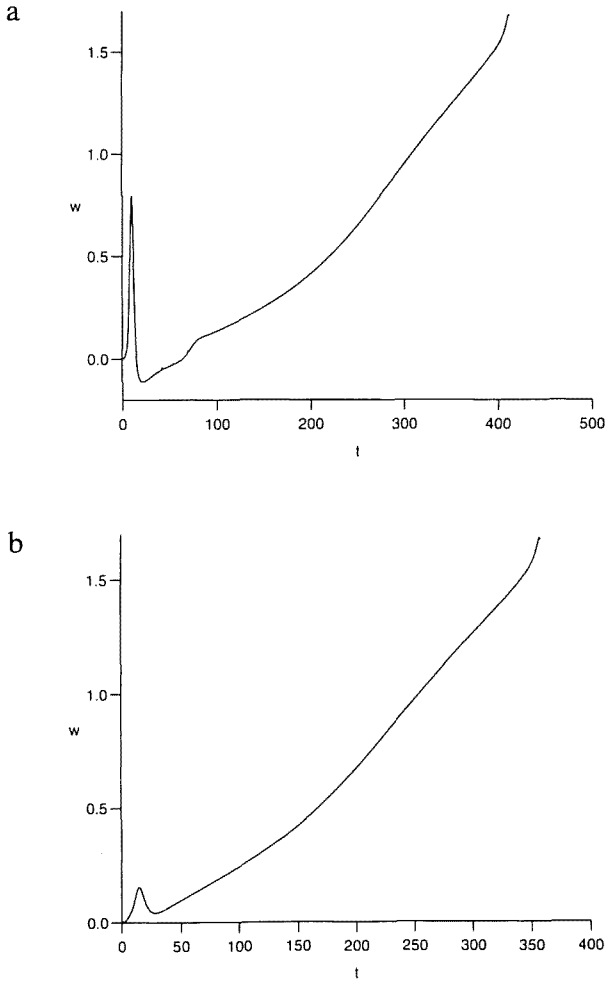

Fig. 4. Plots of wave speed, w, against time for (a) $v_0 = 6000$, $\sigma = 16.7$ and (b) $v_0 = 2000.0$, $\sigma = 13.0$.

ahead of the oxidation front means that the front is propagating into a mixture in which the concentration of the inhibitor v is falling with time – mathematically any sharp front wave will be obtained as a constant velocity solution of eq. (4a) parametrised by the instantaneous value of v ahead of the front region.

3.4. WAVE PROFILES

The evolution of the concentration profiles when a travelling wave is initiated is shown in Fig. 5(a, b), where we plot u and v, respectively, against x for increasing t, with the time increment between each profile being constant. Fig. 5(a) shows the rapid, autocatalytic increase of u in the initiation region followed by a series of profiles which appear to be self-similar in shape. There is a discernable increase in the spatial distance between these profiles as t increases in line with the comments made above that the calculated wave velocity does not approach a constant value. Ahead of the wave, u attains a very small and slightly increasing value (which cannot be seen on the scale of the plot in Fig. 5(a)). The final profile shown in Fig. 5(a) is the one just after the clock reaction has taken over with the value of u ahead of the wave rising rapidly.

A similar picture can be seen in Fig. 5(b). The initial depletion of $[Br^-]$ in the initiation region spreads out from this region as the travelling wave propagates. The value of v ahead of the wave falls rapidly until the critical bromide ion concentration is reached and the clock reaction takes over.

These figures are in contrast to those shown in Fig. 6(a,b,c), where the wave propagation is suppressed. Here, there is an initial rise in u in the initiation region, but now $[Br^-]$ back-fills into this region (Fig. 6(b,c)) inhibiting the autocatalytic growth of $[HBrO_2]$, the concentration of which then falls to low values and remains at $u \approx q$ until the clock reaction occurs. There is still some small effect of the initiation process seen in that v falls to its critical value in the region slightly ahead of the rest of the region, allowing rapid autocatalytic growth in u before the clock reaction takes over and u attains its final value of unity everywhere in the domain, (Fig. 6(a)).

3.5. CIRCULAR AND SPHERICAL GEOMETRIES

The failure or successful initiation of a reaction-diffusion front depending on the parameters σ and v_0 can be determined for circular or spherically-symmetric systems in exactly the same way as described above, employing the modified form of the Laplacian operator. The dependence of the critical radius σ_{cr} on the initial bromide ion concentration v_0 for a circle and a sphere is also shown in Fig. 2(a), with the $v_0^{1/4}$ plot shown in Fig. 2(b). In general, the critical radius for a sphere exceeds that for a circle, which, in turn, exceeds that for the planar case, for equal values of v_0. This indicates that waves are increasingly hard to initiate as the dimension of the system increases. Such a result can be expected from the increasing facil-

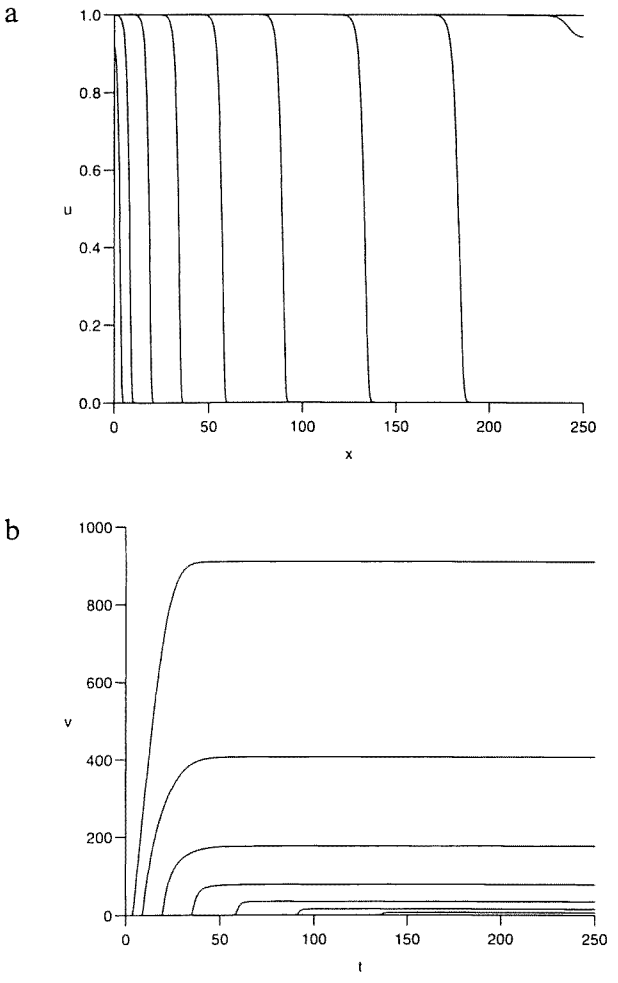

Fig. 5. Concentration profiles of (a) u and (b). v plotted against x, depicting initiation of the travelling front for $v_0 = 2000$ and $\sigma = 13.0$.

ity for diffusion of the inhibitor species as the geometry changes (the curvature becomes increasingly more positive as we move from plane to circular to spherical wave from the point of view of the bromide ion – it becomes increasingly more negative from the point of view of the autocatalytic species).

The slopes of the apparently linear dependences of σ_{cr} on $v_0^{1/4}$ are of interest, being approximately 0.5, 0.35 and 0.29 in Fig. 2(b) for plane, circular and spherical geometries, respectively (for large v_0). On the basis of diffusion alone, we would expect these to be in the ratio $1 : 1/\sqrt{2} : 1/\sqrt{3}$, acting as confirmation of the diffusion- only theory developed in the appendix.

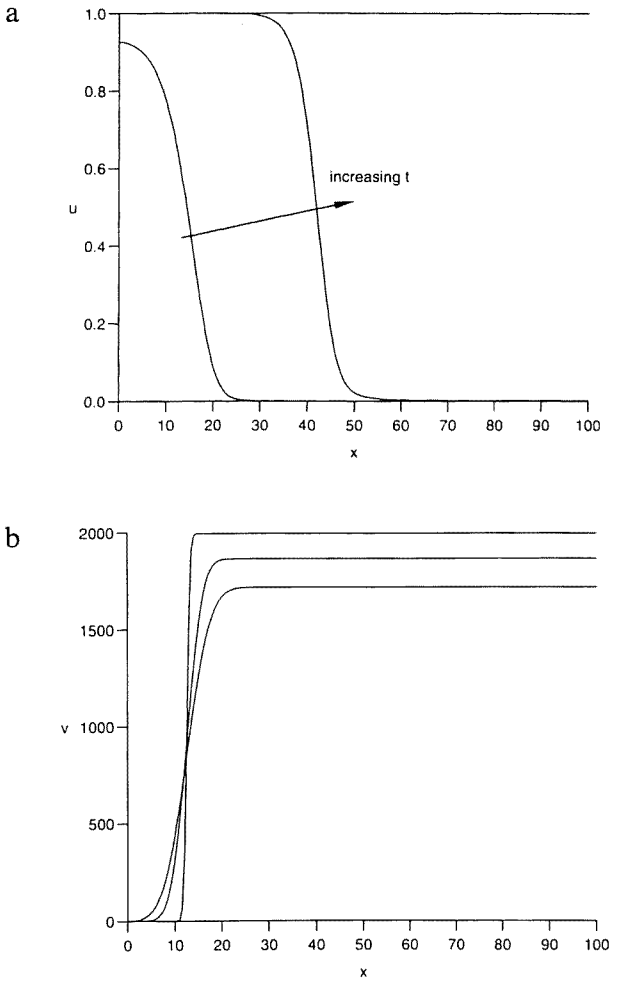

Fig. 6. Concentration profiles of u and v depicting suppression of a travelling front for $v_0 = 2000$, $\sigma = 12.5$ (a) depicts the development of the u profile, (b) and (c) show the initial and longer time developments, respectively, of the v profile. *Fig. 6 continued on next page.*

4. Discussion and conclusion

The analysis presented above indicates the likely existence of critical conditions for the successful initiation of a reaction– diffusion wave in the bromate–ferroin reaction – a typical example of a chemical system with isothermal feedback kinetics. There are, thus, strong parallels with the situation in which feedback arises via a thermal mechanism (i.e. flames) and where species diffusion is replaced by thermal diffusion (conduction of heat from the reaction zone into cold reactants ahead of the flame front). The numerics suggest that a constant velocity wave is unlikely to evolve in the finite time between initiation and the homogeneous clock

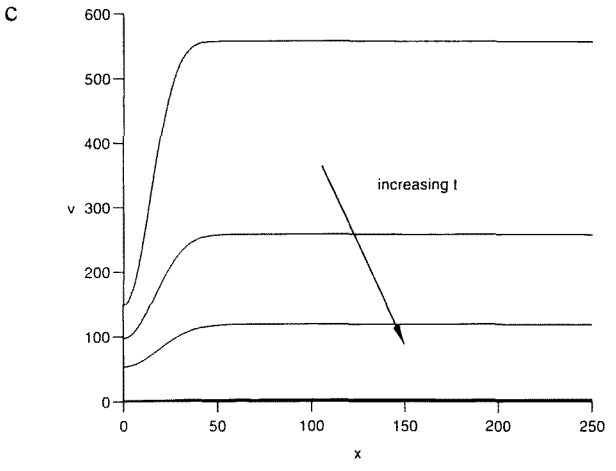

Fig. 6 (continued).

reaction, even for systems in which the initial bromide ion concentration is quite large (long clock times) as, in the that case, the critical initiation radius is also quite large. A scaling of σ_{cr} with $v_0^{1/4}$ has been suggested and appears to hold at large values of v_0.

For a more quantitative test, the dimensionless groups σ and v_0 need to be converted back into dimensional quantities. Using the known values of the reaction rate constants, typical values of the initial reactant concentrations taken from Showalter [1] and a value of $D_u = 2 \times 10^{-5}\,\mathrm{cm^2\,s^{-1}}$, we obtain the following conversion factors:

$$r = \sqrt{\frac{D}{k_5 A H}} \times \sigma \approx 5 \times 10^{-3}\ \mathrm{cm} \times \sigma, \tag{8a}$$

$$[\mathrm{Br}^-]_0 = \frac{k_5 A}{k_2} \times v_0 \approx 1.4 \times 10^{-6}\mathrm{M} \times v_0 \tag{8b}$$

taking $A = [\mathrm{BrO_3^-}]_0 \approx 0.1\mathrm{M}$ and $H = [\mathrm{H^+}]_0 \approx 0.2\mathrm{M}$, with $k_5 = 42\mathrm{M^{-2}\ s^{-1}}$ and $k_2 = 3 \times 10^6\mathrm{M^{-2}\,s^{-1}}$. Thus, taking $v_0 = 6000$ corresponds to $[\mathrm{Br}^-]_0 = 8.4 \times 10^{-3}\mathrm{M}$ and using $\sigma_{cr} = 16.7$ gives $r_{cr} = 0.84$ mm, i.e. a critical electrode width of 1.68 mm. This prediction is of a similar order of magnitude as the electrodes employed by Showalter in his experimental study, indicating at least a semi- quantitative agreement with the present modelling.

One further experimental point can be rationalised on the basis of the above. If the system is assembled such that an electrode of a fixed radius σ is used with a mixture for which the initial bromide ion concentration exceeds the critical value (as

indicated by the appropriate locus in Fig. 2), then any attempt to initiate a wave will fail. However, the occurrence of Process A will naturally cause the prevailing bulk bromide ion concentration to fall in an approximately first-order manner and at some time later, v will fall to a value equal to $v_{cr}(\sigma)$. The analysis thus predicts a 'delay time' dependent on v_0 for a given constant value of σ. From our previous analysis, the delay time will have a similar dependence on the rate constants and initial reactant concentrations as the clock time, being given in dimensionless terms by

$$t_{\text{delay}} = \frac{\delta}{2q} \ln\left(\frac{v_0}{v_{cr}}\right), \tag{9}$$

obtained by setting $u = q$ in eq. (4b) and ignoring any spatial dependence. Here v_{cr} is the value of v along the critical locus in Fig. 2 appropriate to a particular value of σ. In terms of the actual time t', the delay time will scale in the following way with the initial concentrations:

$$t'_{\text{delay}} \sim \frac{1}{[BrO_3^-]_0[H^+]_0^2} \ln\left\{\frac{[Br^-]_0}{[Br^-]_{cr}}\right\}, \tag{10}$$

where $[Br^-]_{cr}$ refers to the bromide ion concentration corresponding to v_{cr} in terms of the critical loci in Fig. 2. This is precisely the dependence on $[BrO_3^-]_0$, $[H^+]_0$ and $[Br^-]_0$ determined by Showalter in his experiments.

Appendix

The suggested $\sigma_{cr} = O(v_0^{1/4})$ scaling can be estimated on the assumption that the parameters δ and q are small and that v_0 is large. More precisely, following Merkin et al. [3], we put

$$q = q_0\delta^2, \quad v_0 = \delta^{-2}y_0, \tag{A.1}$$

where q_0 and y_0 are both of $O(1)$. Initial conditions then suggest putting

$$u = \delta^2 U, \quad v = \delta^{-2}V, \tag{A.2}$$

and, with x and t left unscaled, for one-dimensional geometry eqs. (4) become

$$U = q_0 + O(\delta), \tag{A.3a}$$

$$\frac{\partial V}{\partial t} = \frac{\partial^2 V}{\partial x^2} + O(\delta). \tag{A.3b}$$

Eq. (A.3a) shows that $u \sim q$ on this time scale. In fact, changes in u occur on a much longer $O(\delta^{-1})$ time scale. Eq. (A.3b) can be solved to get

$$V = \frac{y_0}{\sqrt{\pi}}\left(\sqrt{\pi} - \int_0^{\frac{\sigma+x}{2\sqrt{t}}} e^{-s^2} ds - \int_0^{\frac{\sigma-x}{2\sqrt{t}}} e^{-s^2} ds\right), \quad x < \sigma,$$

$$V = \frac{y_0}{\sqrt{\pi}}\left(\sqrt{\pi} - \int_{\frac{\sigma-x}{2\sqrt{t}}}^{\frac{\sigma+x}{2\sqrt{t}}} e^{-s^2} ds\right), \qquad x > \sigma. \tag{A.4}$$

For $x = 0$, expression (A.4) gives

$$V(0,t) = \frac{2y_0}{\sqrt{\pi}} \int_{\sigma/2\sqrt{t}}^{\infty} e^{-s^2} ds \tag{A.5}$$

with expression (A.5) showing that $V(0,t) \to y_0$ as $t \to \infty$ for σ of $O(1)$. The induction time is, from eq. (7), when t is $O(\delta^{-1})$. Thus, for $V(0,t)$ to remain small on this time scale and allow for the formation of a travelling wave up to the induction time, we must have, from (A.5), σ of $O(\delta^{-1/2})$. Then, from (A.1), we obtain

$$\sigma = O(v_0^{1/4}). \tag{A.6}$$

Similar considerations apply for circular and spherically-symmetric geometries.

References

[1] K. Showalter, J. Phys. Chem. 85 (1981) 440.
[2] V. Gaspar, G. Basza and M.T. Beck, J. Phys. Chem. 89 (1985) 5495.
[3] J.H. Merkin, A.J. Poole, S.K. Scott, J.D.B. Smith and B.W. Thompson, J. Math. Chem. 19 (1996) 15.
[4] R.J. Field, E. Koros and R.M. Noyes, J. Am. Chem. Soc. 94 (1972) 8649.
[5] J.J. Tyson, J. Phys. Chem. 86 (1982) 3006.
[6] J.H. Merkin and D.J. Needham, J. Eng. Math. 23 (1989) 343.